Scientific Research Publishing

Journal of Power and Energy Engineering, 2026, 14(1), 38-66
https://www.scirp.org/journal/jpee
ISSN Online: 2327-5901
ISSN Print: 2327-588X

Numerical Analysis of Key Parameters Influencing the Performance of a PV/T System with Surface-Augmented Forced Air and Nanofluids

Süleyman Karsli[1*], Gökhan Sefer[1], Fevzi Bedir[1], Hüseyin Güllüce[2]

[1]Mechanical Engineering Department, Gebze Technical University, Kocaeli, Türkiye
[2]Atatürk University Technical Sciences Vocational School, Erzurum, Türkiye
Email: *skarsli@gtu.edu.tr

How to cite this paper: Karsli, S., Sefer, G., Bedir, F. and Güllüce, H. (2026) Numerical Analysis of Key Parameters Influencing the Performance of a PV/T System with Surface-Augmented Forced Air and Nanofluids. *Journal of Power and Energy Engineering*, **14**, 38-66.
https://doi.org/10.4236/jpee.2026.141003

Received: December 8, 2025
Accepted: January 26, 2026
Published: January 29, 2026

Copyright © 2026 by author(s) and Scientific Research Publishing Inc.
This work is licensed under the Creative Commons Attribution-NonCommercial International License (CC BY-NC 4.0).
http://creativecommons.org/licenses/by-nc/4.0/

Open Access

Abstract

Photovoltaic/Thermal (PV/T) systems are widely employed as renewable energy solutions in various engineering applications. This study aims to determine the optimal operating conditions and propose enhanced configurations to improve system performance. Numerical simulations were conducted using ANSYS Fluent software to evaluate the effects of various modifications on the PV/T system. To mitigate the adverse impact of elevated operating temperatures on system efficiency, different cooling fluids were employed, including forced air, water, multi-walled carbon nanotube (MWCNT)-water nanofluid, and graphene nanoparticle-water nanofluid. Simulation outcomes—including CFD-generated contour plots, Taguchi optimization results, and performance data derived from energy and exergy analyses—were systematically evaluated and visualized through appropriate graphs. Among the tested fluids, the MWCNT/water nanofluid demonstrated 5% higher total energy efficiency and 0.4% higher exergy efficiency on average compared to the graphene/water mixture. For the MWCNT/water nanofluid, which exhibited the highest exergy efficiency, a multiple regression model was developed as follows: $\eta_{ex} = 9500 - 0.0380 \cdot V_{air} + 0.00961 \cdot I + 0.0042 \cdot V_{air}^2 - 0.000002 \cdot I^2 + 0.000300 \cdot V_{air} \cdot I$. The analysis revealed that increasing the air flow rate consistently improved both the thermal and exergy efficiencies of the system across all tested configurations.

Keywords

PV/T Systems, Energy, Exergy, Optimization, Thermal Systems, CFD Method

1. Introduction

The growing global demand for energy, driven by population increase and industrialization, has intensified interest in renewable and sustainable energy solutions. Among these, solar energy is particularly attractive due to its abundance and environmental benefits [1] [2]. Photovoltaic/Thermal (PV/T) systems have gained attention as hybrid technologies capable of producing both electrical and thermal energy from solar radiation, thereby improving overall system efficiency [3] [4]. A key challenge in PV/T systems is the elevated temperature of photovoltaic (PV) cells, which can exceed 50˚C under high irradiance. This leads to reduced electrical efficiency and may cause permanent damage to the cell structure [5]. To mitigate this, various cooling strategies have been proposed, ranging from conventional fluids to advanced nanofluids [6] [7]. Nano fluids, suspensions of nanoparticles in base fluids, have demonstrated significant potential in enhancing heat transfer. Several studies have reported improved thermal and exergy performance of PV/T systems with nanofluid use. For example, Sardarabadi *et al.* observed a notable increase in both energy and exergy efficiency using SiO_2-water nanofluids [8]. Similarly, Hamoudah and Etaig [9] reported lower PV cell temperatures and enhanced thermal performance with Al_2O_3-water mixtures. Recent works also explored advanced geometries and hybrid nanofluids. Samylingam *et al.* applied CFD and response surface methodology (RSM) to optimize system parameters using MXene-based nanofluids, achieving over 80% energy efficiency [10]. Abdelgaied *et al.* emphasized the role of fin configurations in dual-fluid systems, showing efficiency gains through optimized designs [11].

However, limited research has integrated CFD simulations, nanofluid cooling, surface-enhanced designs, and statistical optimization into a unified analysis. This study addresses this gap by evaluating a PV/T system equipped with forced air flow and serpentine copper tubes—both finned and unfinned—cooled by water, graphene-water, and MWCNT-water nanofluids. The concentration of nanofluids used in the analysis is 0.5%. The thermo-physical properties of MWCNT/water nanofluid are given as follows: density 1600 kg/m^3, thermal conductivity 3000 W/(m·K), and specific heat 0.796 kJ/(kg·K). Similarly, the thermophysical properties of Graphene nanofluid are given as follows: density 2100 kg/m^3, thermal conductivity 5000 W/(m·K), and specific heat 0.710 kJ/(kg·K). In the analysis, these properties for water were taken as density 997 kg/m^3, thermal conductivity 0.607 W/(m·K), and specific heat 4.180 kJ/(kg·K), respectively [3]. Simulations were conducted using ANSYS Fluent, and results were optimized using Taguchi and regression analyses to determine ideal operating conditions.

2. Computational Fluid Dynamics (CFD) Analysis in PV/T Systems

Computational Fluid Dynamics (CFD) is a highly precise analytical technique that simulates fluid flow phenomena using numerical methods and databases. When modeling PV/T (Photovoltaic/Thermal) systems with CFD, the Navier-Stokes

conservation equations are employed to accurately resolve flow dynamics in accordance with the system's geometry. The three-dimensional Navier-Stokes equations used in the analysis are summarized below [12] [13]:

Mass Conservation Equation:

$$\frac{\partial p}{\partial t}+\frac{\partial u}{\partial x}+\frac{\partial v}{\partial y}+\frac{\partial w}{\partial z}=0 \tag{1}$$

Momentum Conservation Equation:

1) in the x-direction

$$\frac{\partial u}{\partial t}+div\left(u\cup\right)=-\frac{1}{\rho}\frac{\partial p}{\partial x}+\mu div\left(gradu\right)+\rho\overline{g_x} \tag{2}$$

2) in the y-direction

$$\frac{\partial v}{\partial t}+div\left(v\cup\right)=-\frac{1}{\rho}\frac{\partial p}{\partial y}+\mu div\left(gradv\right)+\rho\overline{g_y} \tag{3}$$

3) in the z-direction

$$\frac{\partial w}{\partial t}+div\left(w\cup\right)=-\frac{1}{\rho}\frac{\partial p}{\partial z}+\mu div\left(gradw\right)+\rho\overline{g_z} \tag{4}$$

These conservation equations are solved numerically using finite volume-based codes in CFD. The CFD workflow involves:

1) Defining the PV/T system geometry.

2) Generating a mesh structure.

3) Simulating flow dynamics within the system.

4) Assigning fluid properties and boundary conditions to the geometry.

To account for turbulence effects, the Reynolds-Averaged Navier-Stokes (RANS) equations were employed. Among the various turbulence models available in commercial CFD software, the SST k-omega model was selected for this study. This model combines the strengths of the k-epsilon (k-ε) and omega (ω) models, providing more accurate predictions of turbulent flow behavior [14] [15]. The SST k-omega model accurately captures viscous friction effects, particularly in the viscous sublayer of turbulence. It also performs well in the free-stream region and can provide more accurate results in flows with reverse pressure gradients. When performing CFD analysis with the coil cooling system added to PV/T systems, an appropriate mathematical model must be created, and this mathematical model must also include fluid dynamics equations, energy equations, and turbulence models. The SST-k omega model preferred in the analysis contains equations that comprehensively address the physical behaviour of the system [13].

2.1. System Specifications

The PV/T system under investigation has the following dimensions:

Overall dimensions: 675 mm × 380 mm × 17.3 mm.

Absorber plate: 675 mm × 380 mm × 0.7 mm (thickness).

Serpentine pipe material: Copper.

Pipe dimensions: Outer diameter: 10 mm; Inner diameter: 8 mm; Total length: 280 cm.

The serpentine pipe is positioned within the air duct beneath the PV/T panel. Figures 1-5 illustrate the serpentine design, including cross-sectional and isometric views of both finned and finless configurations.

2.2. Mesh Structure

Different mesh types were applied to accommodate the system's layered structure:

Tetrahedral mesh: Used for solid structures and the working fluid.

Hexahedral mesh: Applied to the forced air region.

As shown in Figures 2-5, the mesh resolution was as follows:

Finless serpentine: 1,507,318 cells.

Finned serpentine: 2,194,180 cells.

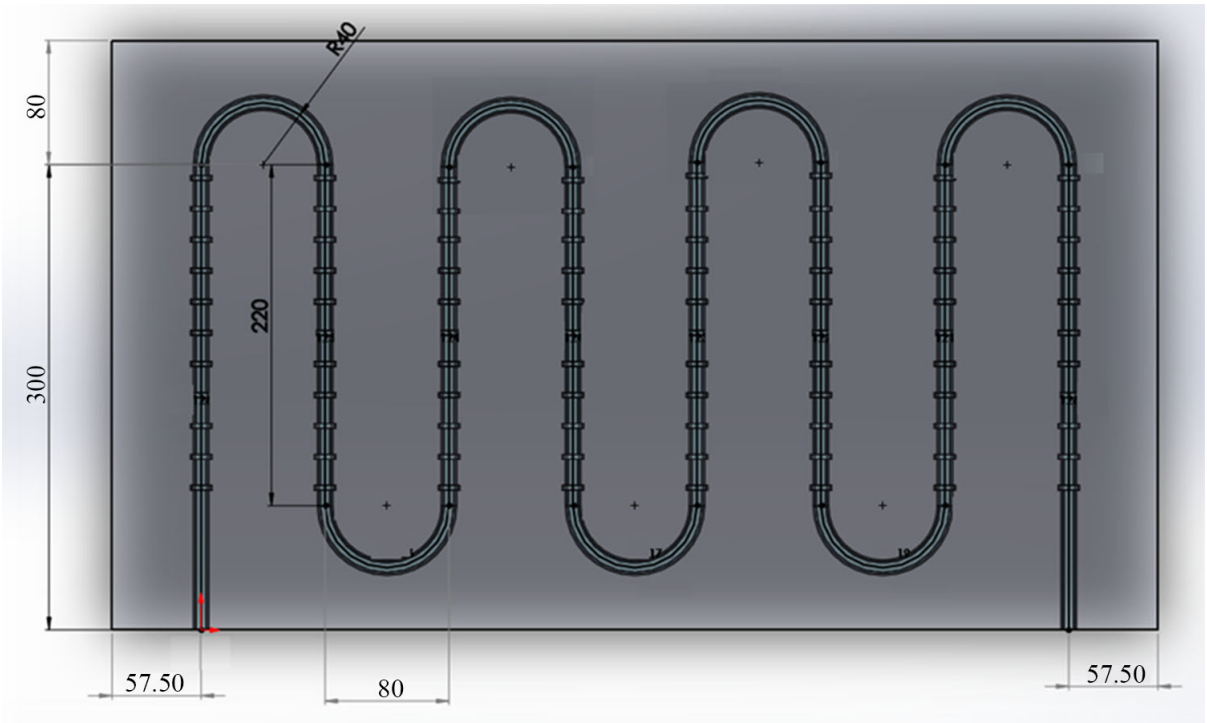

Figure 1. Serpentine and fins.

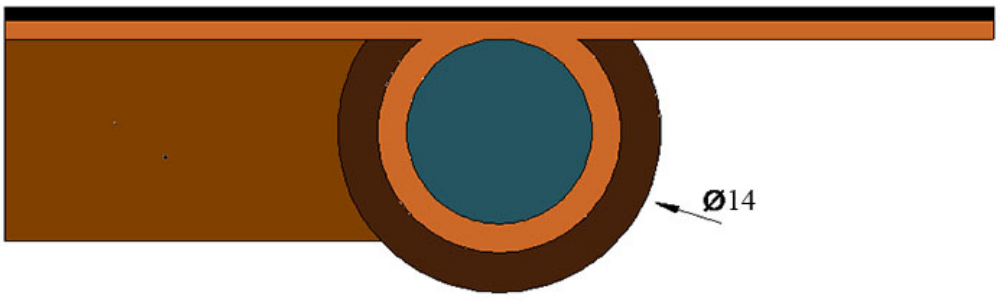

Figure 2. Cross-sectional view of fin.

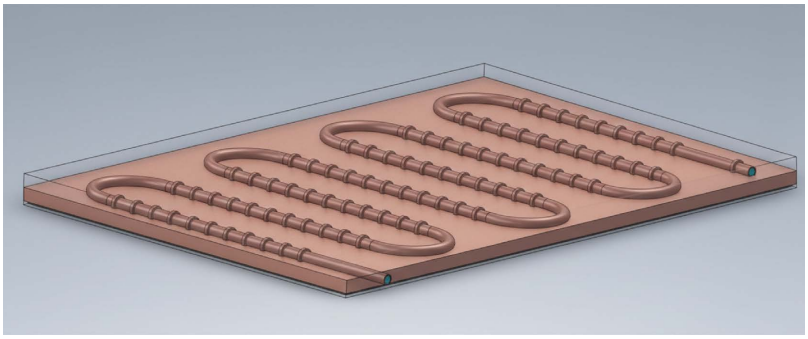

Figure 3. Isometric view of the finned serpentine.

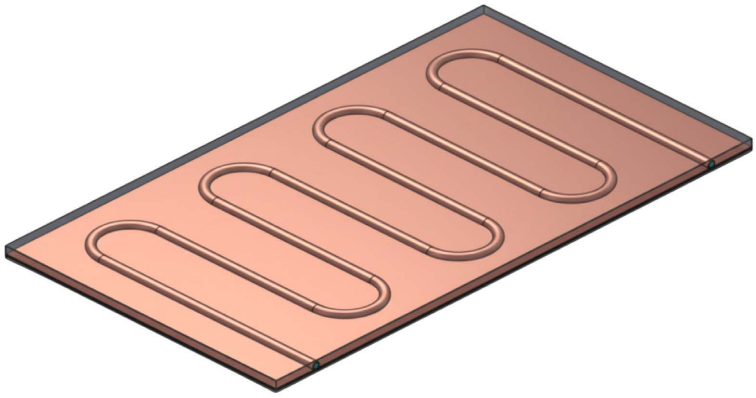

Figure 4. Isometric view of the finless serpentine.

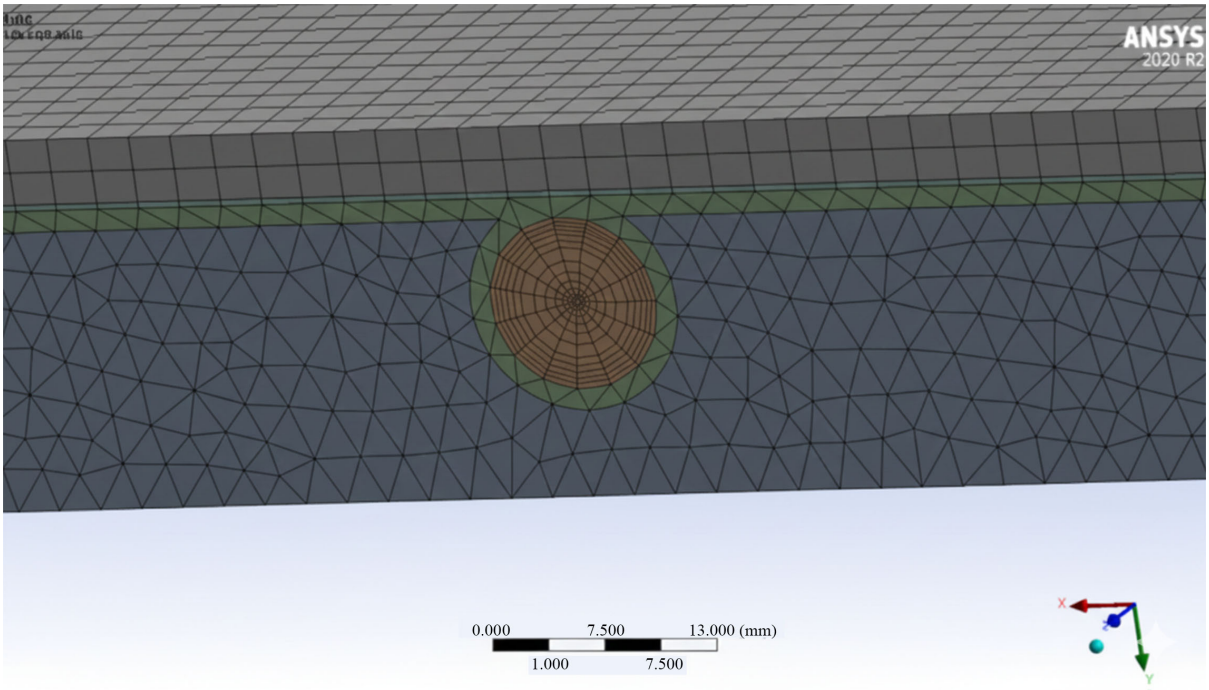

Figure 5. Network structure in the modeled system.

3. Energy and Exergy Analysis

The total energy output of a PV/T panel is the sum of the thermal energy emitted, the electrical energy generated, and the power loss associated with the process. Mathematically, this can be expressed as:

$$\dot{E}_{out} = \dot{Q}_U + \dot{E}_{elec} + \dot{E}_{loss} \tag{5}$$

where:

$\dot{E}_{loss}$: Represents the power dissipated from the PV/T panel to the environment due to the temperature difference between the panel and its surroundings.

$\dot{Q}_U$: Denotes the useful thermal power absorbed by the working fluid from the panel's bottom surface.

3.1. Useful Thermal Power ($\dot{Q}_U$)

The thermal power can be calculated using:

$$\dot{Q}_U = \dot{m} * c_p * \left(T_o - T_i\right) \tag{6}$$

where:

$\dot{m}$ = Mass flow rate of the working fluid;

c_p = Specific heat at constant pressure;

T_i and T_o = Inlet and outlet temperatures of the fluid, respectively.

3.2. Electrical Power Output ($\dot{E}_{elec}$)

The electrical energy generated by the PV/T panel is given by:

$$\dot{E}_{elec} = V_{oc} * I_{sc} * FF \tag{7}$$

where:

V_{oc} = Open circuit voltage;

I_{sc} = Short circuit current;

FF = Fill factor, representing the panel's maximum power conversion efficiency.

$$FF = \frac{P_m}{V_{oc} * I_{sc}} \tag{8}$$

where, P_m is the maximum electrical output power, calculated as:

$$P_m = V_m * I_m \tag{9}$$

Here, V_m and I_m are the voltage and current at the maximum power point (MPP). Thus, the electrical power can also be expressed as:

$$\dot{E}_{elec} = P_m = V_m * I_m \tag{10}$$

Energy input ($\dot{E}_{in}$):

The energy input to the PV/T panel is determined by the total solar irradiance $I_{(t)}$ incident on the panel's surface area A_p :

$$\dot{E}_{in} = I_{(t)} * A_p \tag{11}$$

3.3. Energy Efficiency ($\eta_{PV/T}$)

The overall energy efficiency of the PV/T system is the ratio of useful output energy to the total input energy:

$$\eta_{PV-T} = \frac{\dot{E}_{out}}{\dot{E}_{in}} = \frac{\dot{Q}_U + \dot{E}_{elec}}{\dot{E}_{in}} \tag{12}$$

The overall energy efficiency of the PV/T system is the ratio of useful output energy to the total input energy:

$$\eta_{PV-T} = \frac{\dot{Q}_U}{\dot{E}_{in}} + r * \frac{\dot{E}_{elec}}{\dot{E}_{in}} = \eta_{th} + r * \eta_{elec} \tag{13}$$

where:

r = Packing factor (ratio of the PV cell area $A_{PV/T}$ to the panel area A_P);

r = 0: No PV cells in the panel;

r = 1: Entire panel area covered by PV cells.

The packing factor is calculated as:

$$r = \frac{A_{PV-T}}{A_P} \tag{14}$$

For the PV/T system in this study, which includes an air flow duct and a serpentine coil for fluid circulation, the thermal efficiency is:

$$\eta_{th} = \frac{\dot{m}_f * c_{p,f} * \left(T_{f,out} - T_{f,in}\right) + \dot{m}_{air} * c_{p,air} * \left(T_{air,out} - T_{air,in}\right)}{I_{(t)} * A_P} \tag{15}$$

3.4. Exergy Analysis

Exergy efficiency reflects the quality of energy conversion from solar energy and is defined as:

$$\varepsilon_{PV\_T} = \frac{\dot{E}x_{out}}{\dot{E}x_{in}} \tag{16}$$

where the total exergy output ($\dot{E}x_{out}$) includes electrical exergy and thermal exergy:

$$\dot{E}x_{out} = \dot{E}_{xelec} + \dot{Q}_{U,total} \tag{17}$$

Expanding this for the working fluid and air:

$$\begin{aligned} \dot{E}x_{out} = I_0 * V_0 + \dot{m}_f * c_{p,f} \left[\left(T_{f,out} - T_{f,in}\right) - T_{ambient} * \left\langle \ln\left(\frac{T_{f,out}}{T_{f,in}}\right) - R_f * \ln\left(\frac{P_{f,out}}{P_{f,in}}\right) \right\rangle \right] \\ + \dot{m}_{air} * c_{p,air} \left[\left(T_{air,out} - T_{air,in}\right) - T_{ambient} * \left\langle \ln\left(\frac{T_{air,out}}{T_{air,in}}\right) - R_{air} * \ln\left(\frac{P_{air,out}}{P_{air,in}}\right) \right\rangle \right] \end{aligned} \tag{18}$$

where:

$P_{f,out}$ and $P_{air,out}$ = Outlet pressures of the fluid and air;

$P_{f,in}$ and $P_{air,in}$ = Inlet pressures;

R_f and R_{air} = Gas constants for the fluid and air.

The exergy input to the system is derived from solar radiation:

$$\dot{E}x_{in} = I_{(t)} + A_P * \left[1 - \frac{4}{3} * \left(\frac{T_0}{T_{sun}}\right) + \frac{1}{3} * \left(\frac{T_0}{T_{sun}}\right)^4\right] \tag{19}$$

where:

T_0 = Ambient temperature;

T_{sun} = Sun's surface temperature (5777 K in exergy analysis).

Using Jeter's equation [3] [16] [17], the solar exergy input simplifies to:

$$\dot{E}x_{sun} = \left[1 - \left(\frac{T_0}{T_{sun}}\right)\right] * I_{(t)} \tag{20}$$

4. Results

4.1. CFD Analysis Results

4.1.1. PV/T Contours without Flow

This section presents the temperature contours of the PV/T panel under no-flow conditions for solar radiation levels of 200, 400, 600, and 1000 [W·m^{-2}]. Figure 6 and Figure 7 illustrate that the panel's surface temperature increases with higher solar irradiance, as expected due to greater thermal energy absorption.

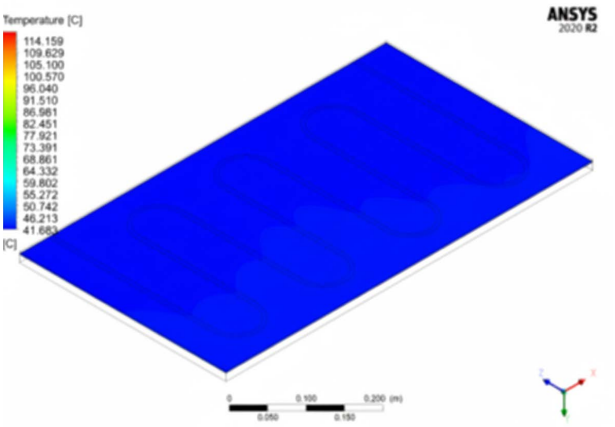

Figure 6. PV-T panel temperature distribution without flow for 200 [W·m^{-2}].

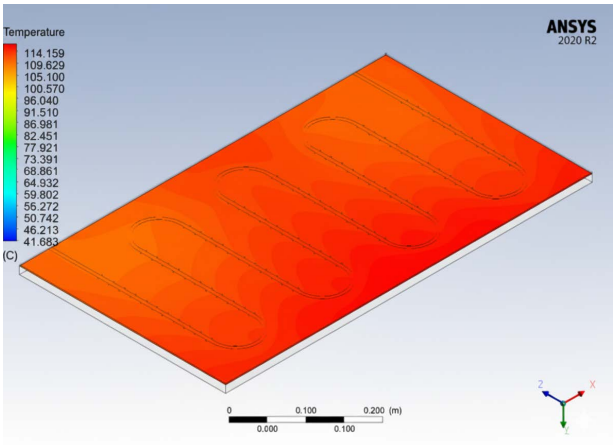

Figure 7. PV-T panel temperature distribution without flow for 1000 [W·m^{-2}].

The temperature gradient is more pronounced at higher irradiance, highlighting the need for effective cooling mechanisms in high-sunlight conditions.

4.1.2. PV/T Panels with Flow and Finless Serpentine

Temperature contours for the PV/T system with a finless serpentine and forced flow are analyzed for nanofluid, which achieves the best cooling, attributed to its superior thermal conductivity (Figures 8-18).

Cooling Performance: MWCNT/water under varying solar irradiance and with working fluids (water, graphene nano platelets, and MWCNT/water).

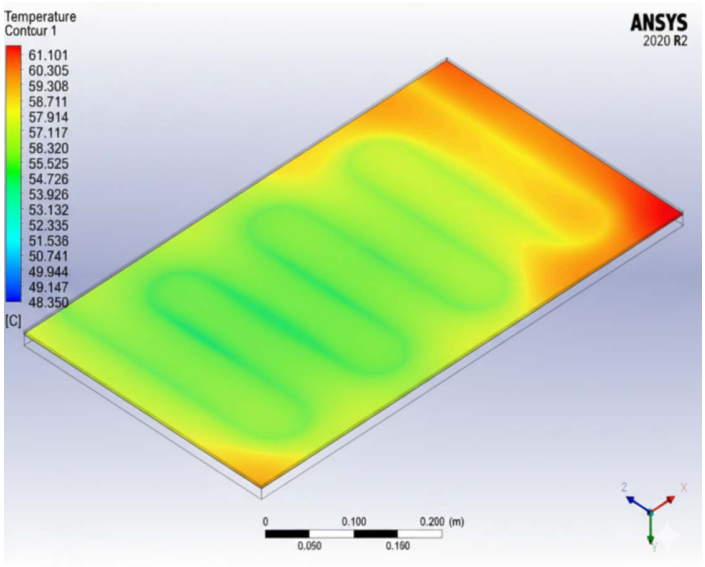

Figure 8. PV-T panel with flow and finless serpentine temperature contour obtained at air velocities of 1 [m·s^{-1}] for the working fluid water and 200 [W·m^{-2}].

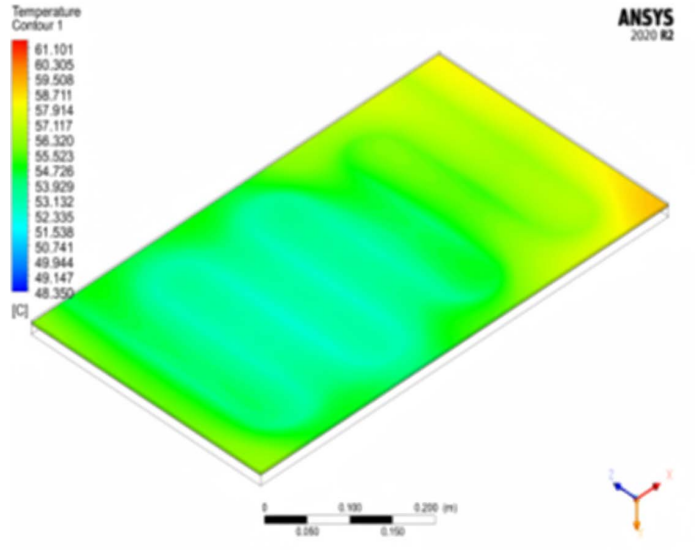

Figure 9. PV-T panel with flow and finless serpentine temperature contour obtained at air velocities of 1 [m·s^{-1}] for the working fluid graphene nano platelet and 200 [W·m^{-2}].

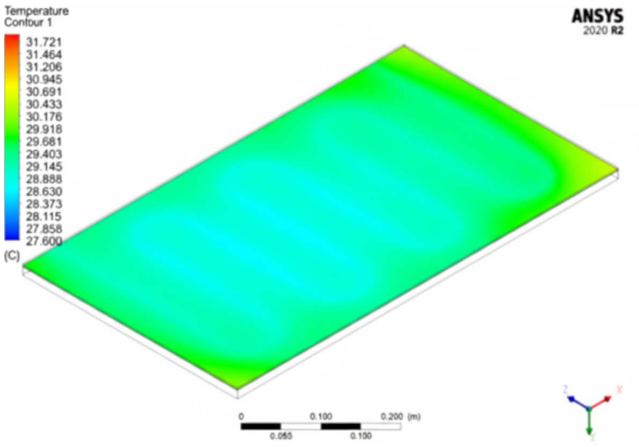

Figure 10. PV/T panel with flow and finless serpentine temperature contour obtained at air velocities of 1 [m·s^{-1}] for the working fluid MWCNT-water and 200 [W·m^{-2}].

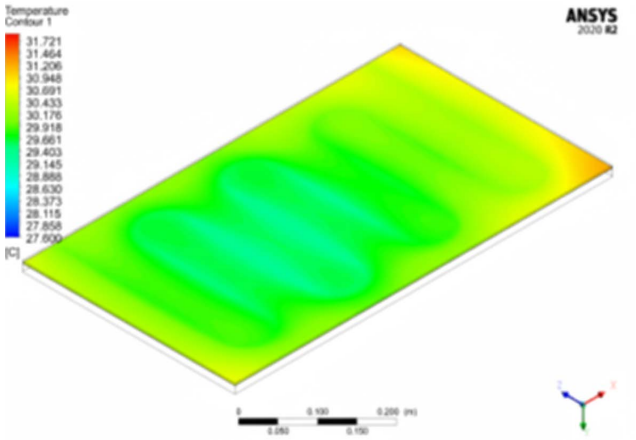

Figure 11. PV-T panel with flow and finless serpentine temperature contour obtained at air velocities of 5 [m·s^{-1}] for the working fluid water and 200 [W·m^{-2}].

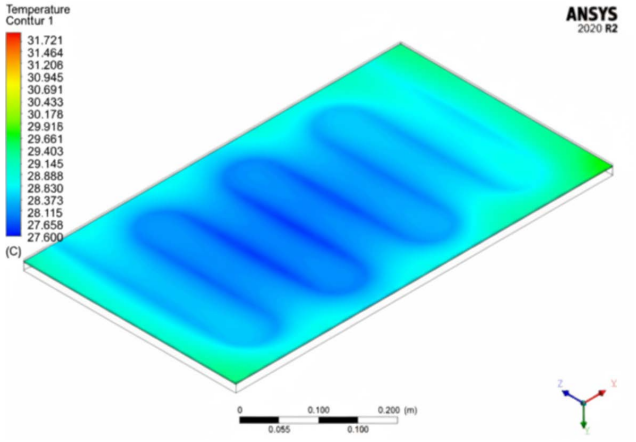

Figure 12. PV-T panel with flow and finless serpentine temperature contour obtained at air velocities of 5 [m·s^{-1}] for the working fluid graphene nano platelet and 200 [W·m^{-2}].

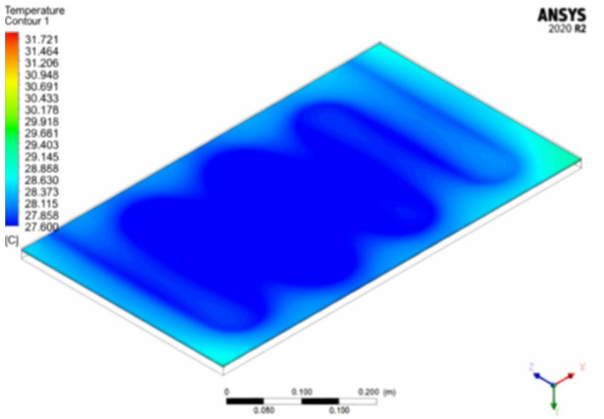

Figure 13. PV-T panel with flow and finless serpentine temperature contour obtained at air velocities of 5 [m·s^{-1}] for the working fluid MWCNT-water and 200 [W·m^{-2}].

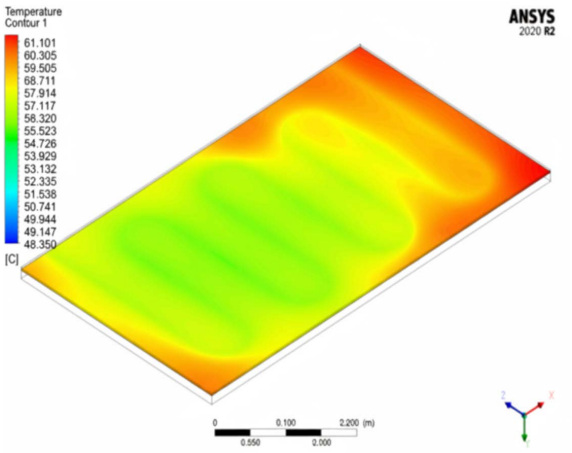

Figure 14. PV-T panel with flow and finless serpentine temperature contour obtained at air velocities of 1 [m·s^{-1}] for the working fluid water 1000 [W·m^{-2}].

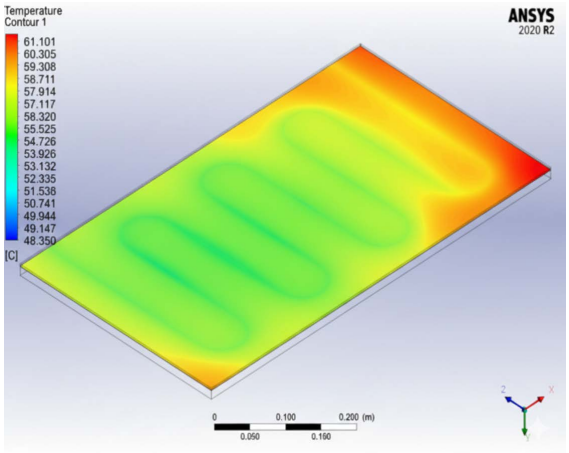

Figure 15. PV-T panel with flow and finless serpentine temperature contour obtained at air velocities of 1 [m·s^{-1}] for the working fluid graphene nano platelet 1000 [W·m^{-2}].

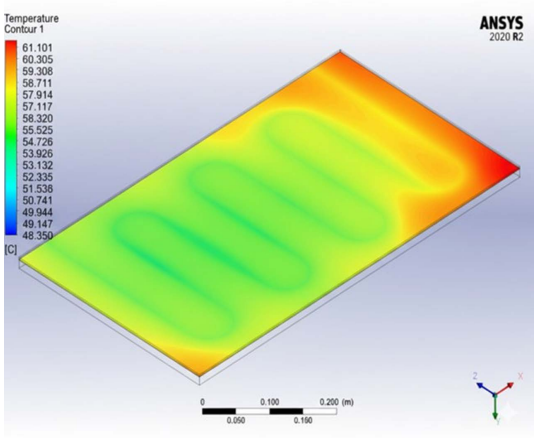

Figure 16. PV/T panel with flow and finless serpentine temperature contour obtained at air velocities of 1 [m·s^{-1}] for the working fluid MWCNT/water 1000 [W·m^{-2}].

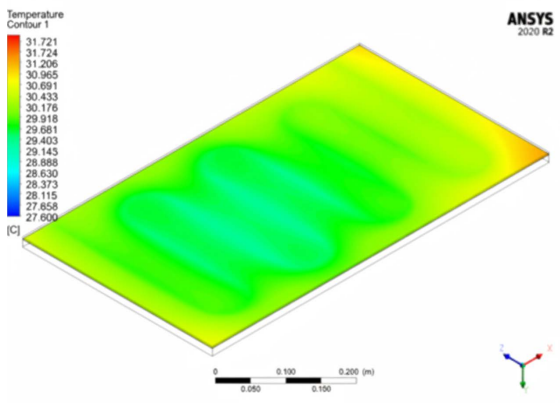

Figure 17. PV-T panel with flow and finless serpentine temperature contour obtained at air velocities of 5 [m·s^{-1}] for the working fluid water 1000 [W·m^{-2}].

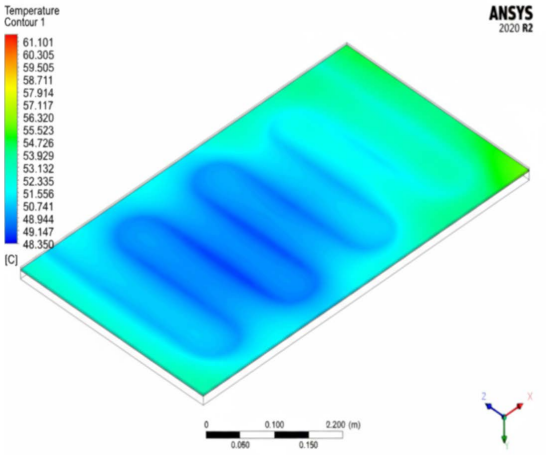

Figure 18. PV-T panel with flow and finned serpentine temperature contour obtained at air velocities of 5 [m·s^{-1}] for the working fluid graphene nano platelet and 1000 [W·m^{-2}].

Air Velocity Impact: Higher air velocity [5 m·s^{-1}] further reduces panel temperatures compared to [1 m·s^{-1}]. The MWCNT/water nanofluid again outperforms other fluids, though temperatures remain higher than at 200 [W·m^{-2}] due to increased solar input. Nanofluids enhance cooling efficiency, with MWCNT/water being the most effective. Higher air velocities amplify this effect.

4.1.3. PV/T Panels with Flow and Finned Serpentine

The finned serpentine design is evaluated under the same conditions as Figures 19-30.

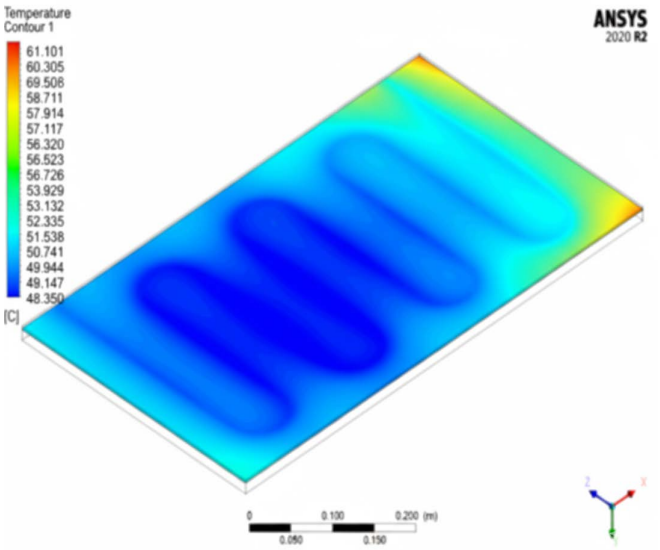

Figure 19. PV-T panel with flow and finned serpentine temperature contour obtained at air velocities of 5 [m·s^{-1}] for the working fluid MWCNT/water and 1000 [W·m^{-2}].

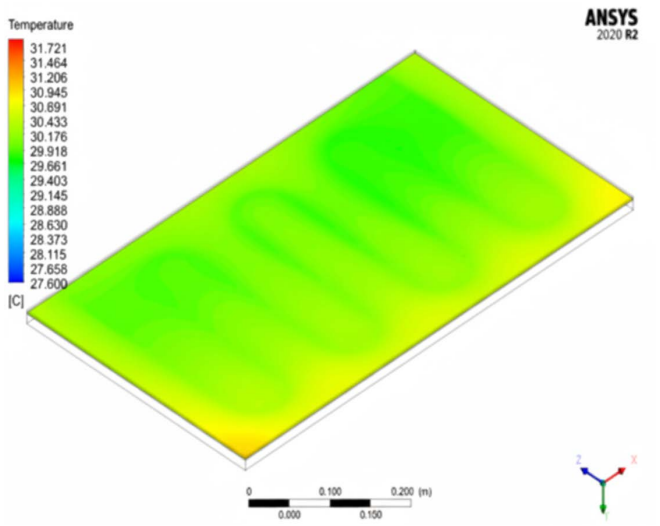

Figure 20. PV-T panel with flow and finned serpentine temperature contour obtained at air velocities of 1 [m·s^{-1}] for the working fluid water and 200 [W·m^{-2}].

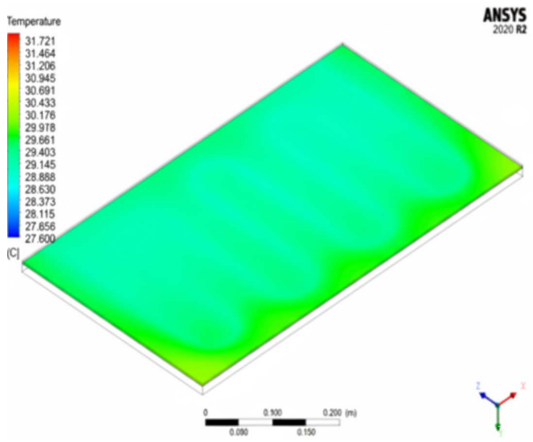

Figure 21. PV-T panel with flow and finned serpentine temperature contour obtained at air velocities of 1 [m·s^{-1}] for the working fluid graphene nano platelet and 200 [W·m^{-2}].

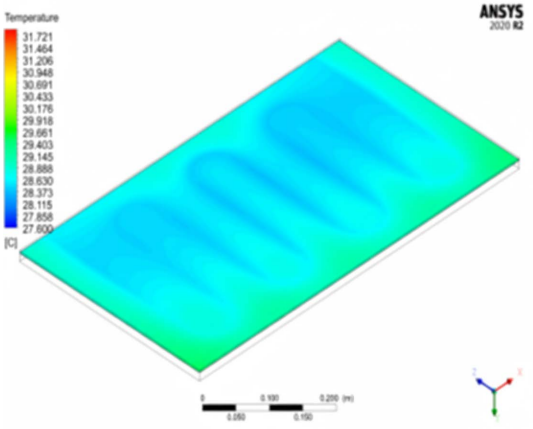

Figure 22. PV-T panel with flow and finned serpentine temperature contour obtained at air velocities of 1 [m·s^{-1}] for the working fluid MWCNT/water 200 [W·m^{-2}].

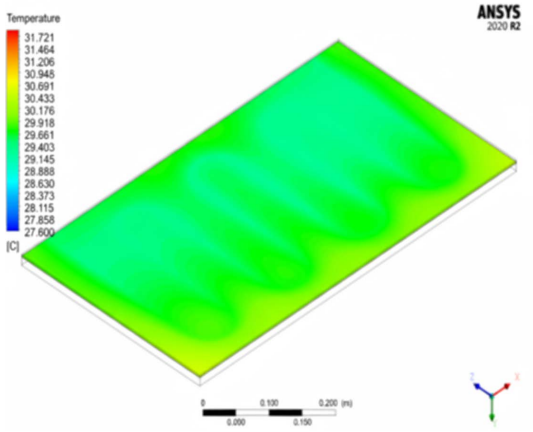

Figure 23. PV-T panel with flow and finned serpentine temperature contour obtained at air velocities of 5 [m·s^{-1}] for the working fluid water and 200 [W·m^{-2}].

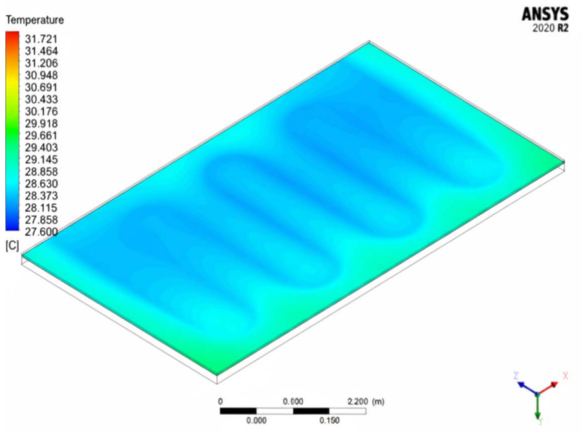

Figure 24. PV-T panel with flow and finned serpentine temperature contour obtained at air velocities of 5 [m·s^{-1}] for the working fluid graphene nano platelet and 200 [W·m^{-2}].

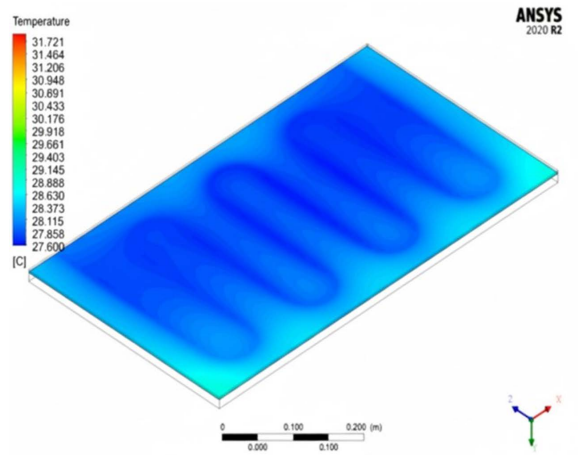

Figure 25. PV-T panel with flow and finned serpentine temperature contour obtained at air velocities of 5 [m·s^{-1}] for the working fluid MWCNT/water and 200 [W·m^{-2}].

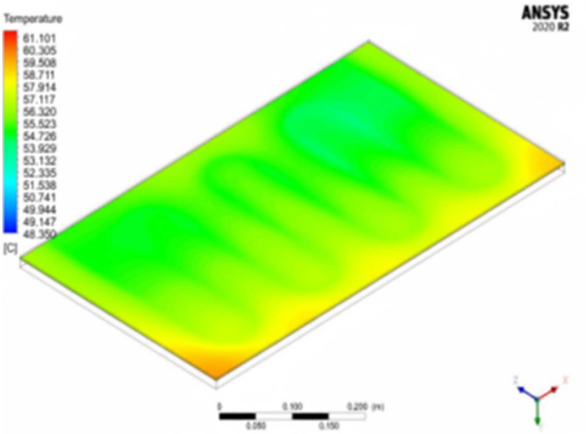

Figure 26. PV-T panel with flow and finned serpentine temperature contour obtained at air velocities of 1 [m·s^{-1}] for the working fluid water 1000 [W·m^{-2}].

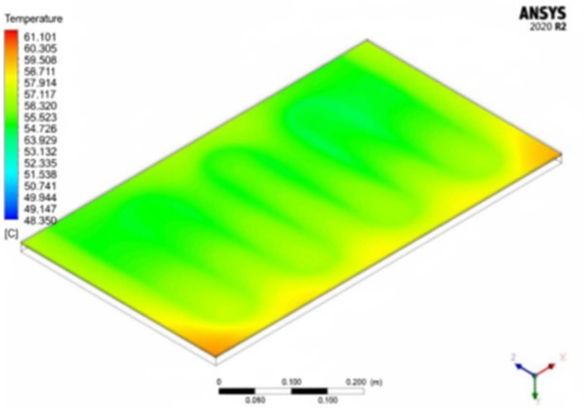

Figure 27. PV-T panel with flow and finned serpentine temperature contour obtained at air velocities of 1 [m·s^{-1}] for the working fluid graphene nano platelet 1000 [W·m^{-2}].

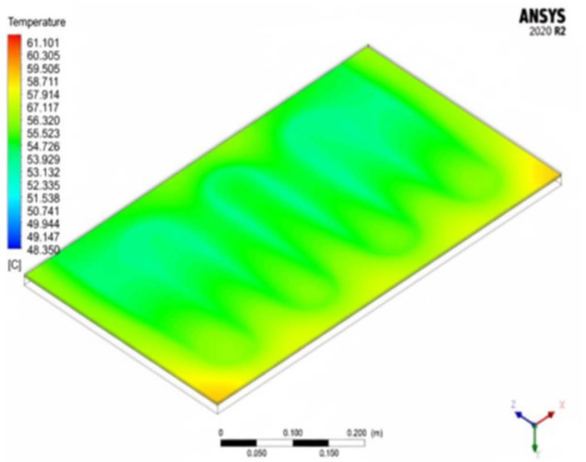

Figure 28. PV-T panel with flow and finned serpentine temperature contour obtained at air velocities of 1 [m·s^{-1}] for the working fluid MWCNT-water 1000 [W·m^{-2}].

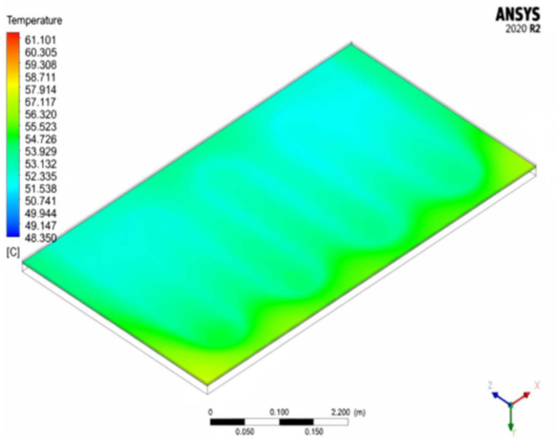

Figure 29. PV-T panel with flow and finned serpentine temperature contour obtained at air velocities of 5 [m·s^{-1}] for the working fluid water 1000 [W·m^{-2}].

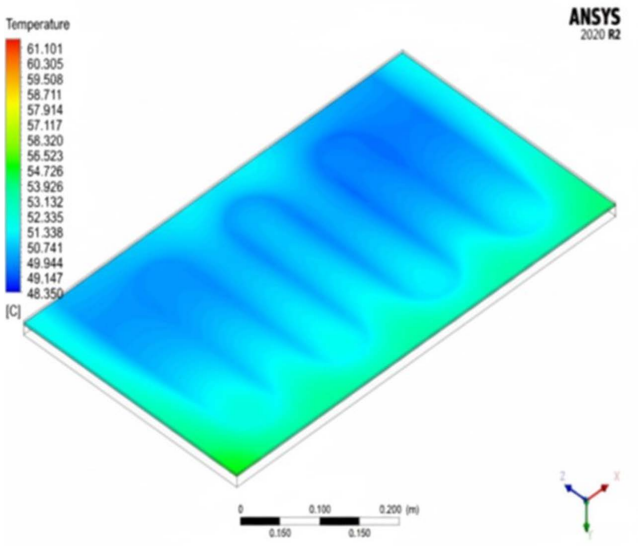

Figure 30. PV-T panel with flow and finned serpentine temperature contour obtained at air velocities of 5 [m·s^{-1}] for the working fluid graphene nano platelet 1000 [W·m^{-2}].

Despite higher baseline temperatures, the finned design with MWCNT/water mitigates temperature spikes effectively. Fins improve heat dissipation, with MWCNT/water maintaining the best performance.

Key Takeaway: Finned configurations consistently outperform finless ones, especially at high irradiance, due to increased surface area for heat transfer.

4.2. Energy and Exergy Analysis Results

Graphical results (Figures 31-42) compare system efficiencies across configurations. The energy and exergy analysis results obtained for the PV/T system are shown in the graphs below. In these graphs, the changes in the total energy and exergy efficiencies of the system for each different configuration condition can be easily observed.

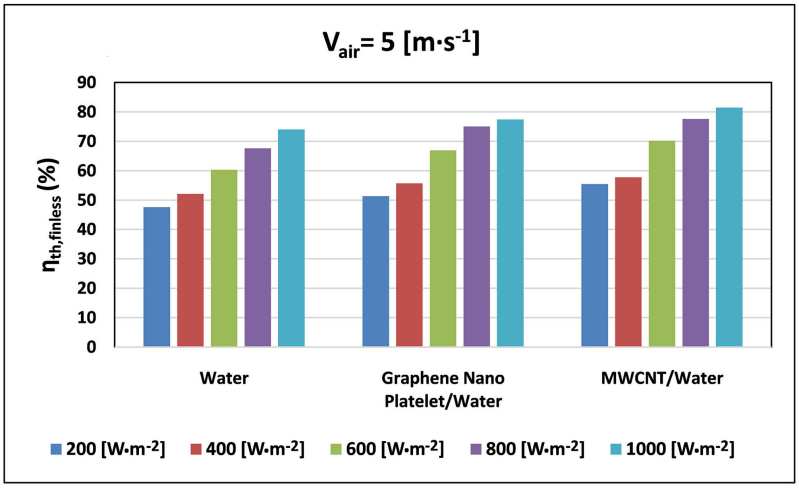

Figure 31. Changes in the total energy efficiency of the system for each fluid flow in the finless serpentine at 5 [m·s^{-1}] air velocity and different solar radiation powers.

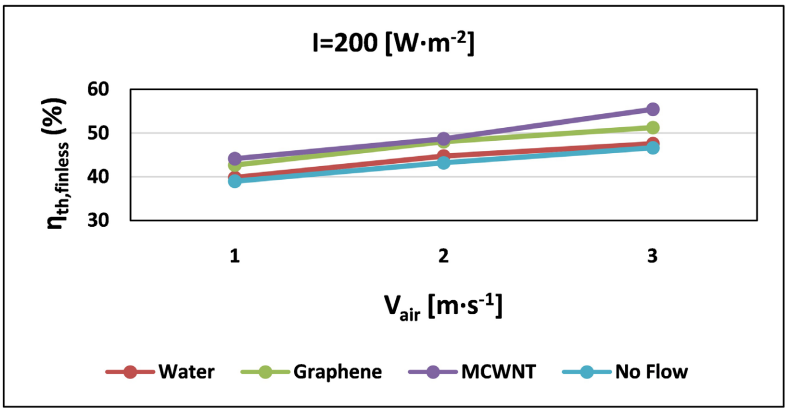

Figure 32. Comparison of the changes in the total energy efficiency of the system for inlet conditions without any flow and flow conditions in the finless serpentine for solar radiation power of 200 [W·m^{-2}].

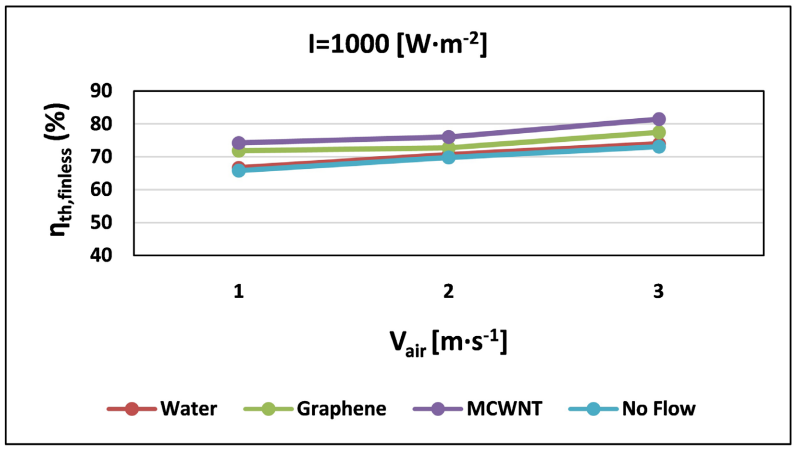

Figure 33. Comparison of the changes in the total energy efficiency of the system for inlet conditions without any flow and flow conditions in the finless serpentine for solar radiation power of 1000 [W·m^{-2}].

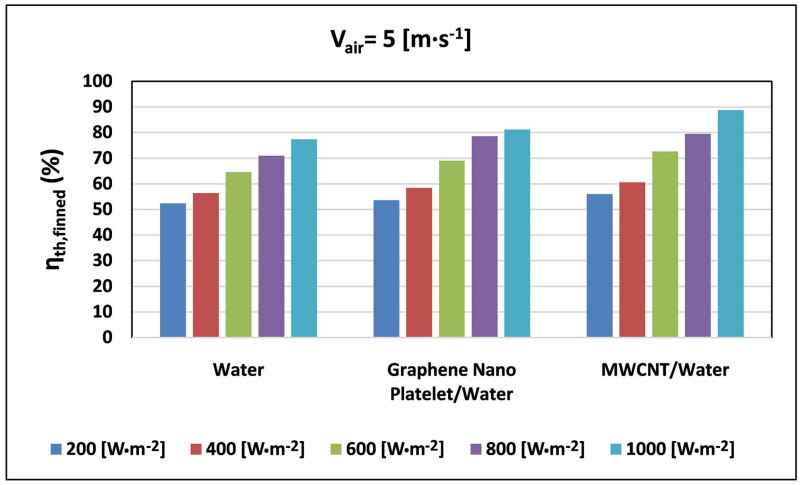

Figure 34. Changes in the total energy efficiency of the system for each fluid flow in the finned serpentine at 5 [m·s^{-1}] air velocity and different solar radiation powers.

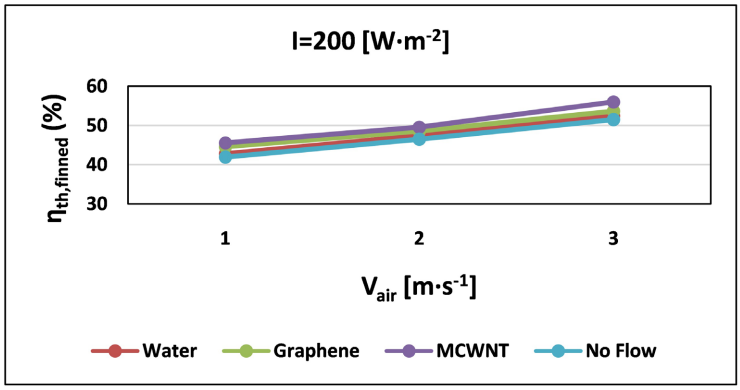

Figure 35. Comparison of the changes in the total energy efficiency of the system for inlet conditions without any flow and flow conditions in the finned serpentine for solar radiation power of 200 [W·m^{-2}].

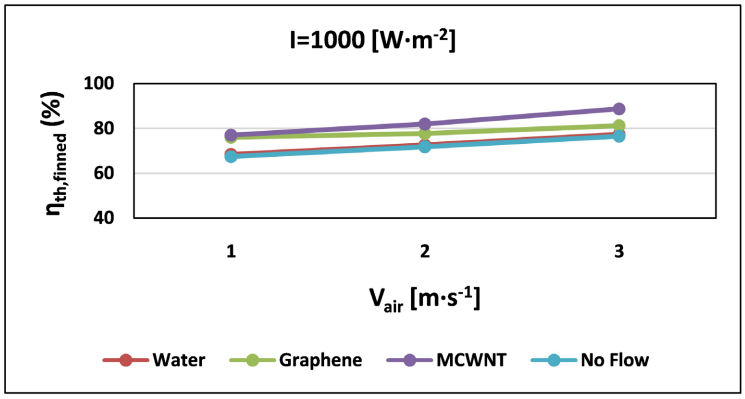

Figure 36. Comparison of the changes in the total energy efficiency of the system for inlet conditions without any flow and flow conditions in the finned serpentine for solar radiation power of 1000 [W·m^{-2}].

Finned vs. Finless: Finned serpentines improve energy efficiency by ~10% on average.

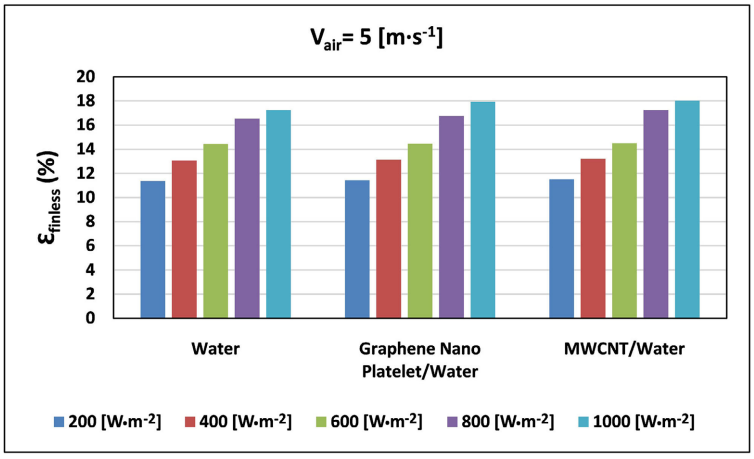

Figure 37. Changes in the total exergy efficiency of the system for each fluid flow in the finless serpentine at 5 [m·s^{-1}] air velocity and different solar radiation powers.

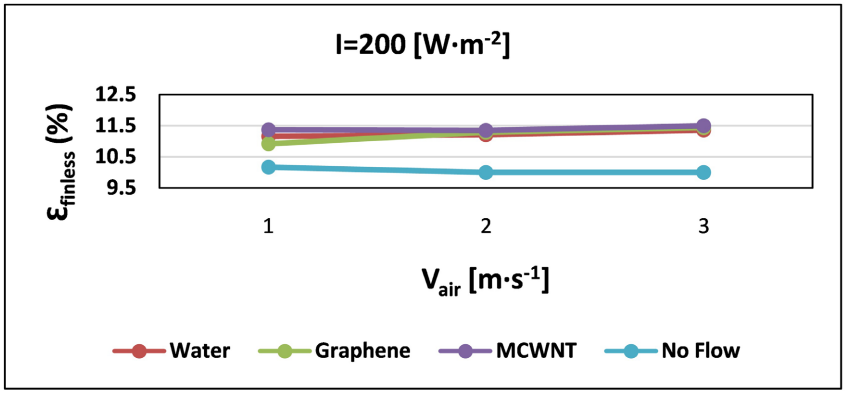

Figure 38. Comparison of the changes in the total exergy efficiency of the system for inlet conditions without any flow and flow conditions in the finless serpentine for solar radiation power of 200 [W·m^{-2}].

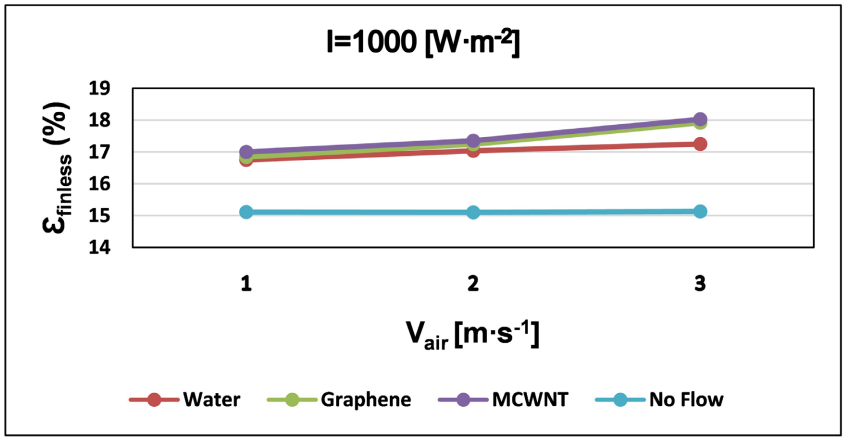

Figure 39. Comparison of the changes in the total exergy efficiency of the system for inlet conditions without any flow and flow conditions in the finless serpentine for solar radiation power of 1000 [W·m^{-2}].

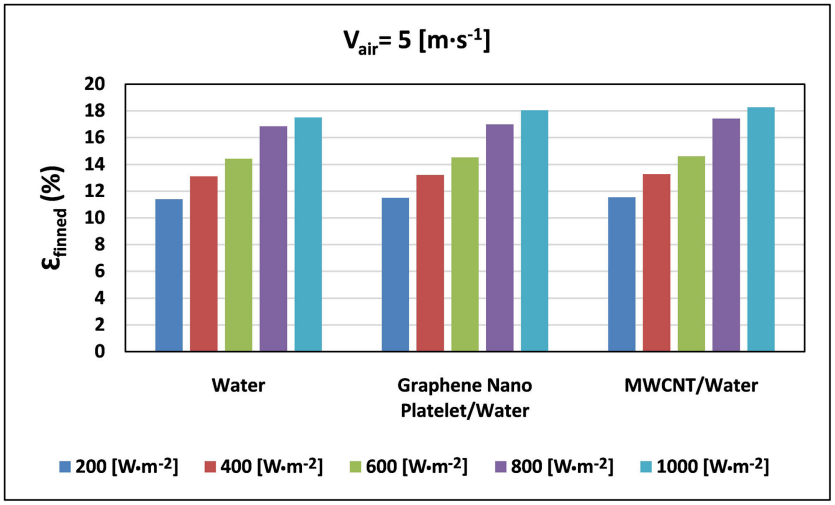

Figure 40. Changes in the total exergy efficiency of the system for each fluid flow in the finned serpentine at 5 [m·s^{-1}] air velocity and different solar radiation powers.

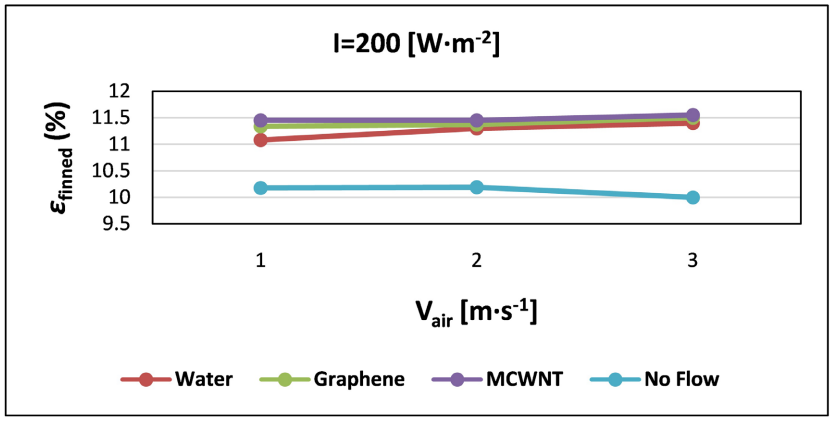

Figure 41. Comparison of the changes in the total exergy efficiency of the system for inlet conditions without any flow and flow conditions in the finned serpentine for solar radiation power of 200 [W·m^{-2}].

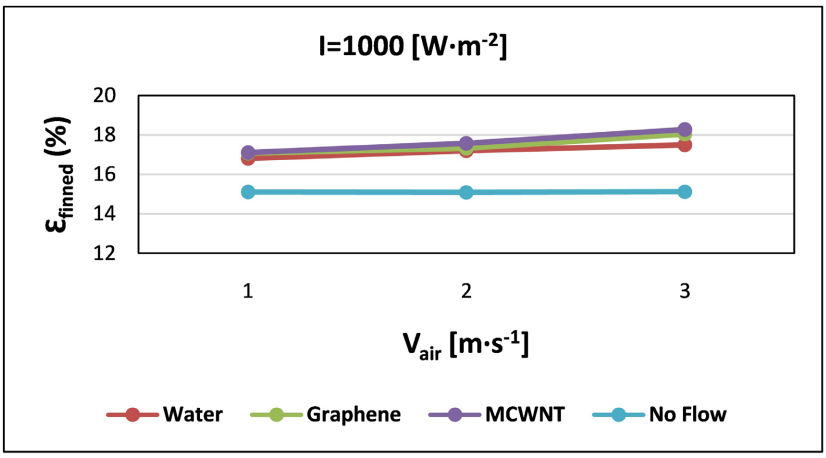

Figure 42. Comparison of the changes in the total exergy efficiency of the system for inlet conditions without any flow and flow conditions in the finned serpentine for solar radiation power of 1000 [W·m^{-2}].

Finned Systems: Show a 0.5% average increase in exergy efficiency.

Nanofluids: MWCNT/water maximizes exergy output, aligning with energy efficiency trends. As a conclusion, combining finned designs with MWCNT/water nanofluid and high air velocity optimizes both energy and exergy performance.

4.3. Comparative Analysis with Literature

Table 1 shows a comparison of the results regarding system effectiveness obtained in this study with similar studies previously conducted in the literature. When this table is examined, there is a good agreement between the results obtained from the analysis where system efficiency was calculated and those in the literature. In general, it is understood that the efficiency of the finned serpentine system using nanofluids is higher than that of other configurations. It is possible to achieve different performance improvements depending on basic parameters such as nanofluid type, finned or finless serpentine design, and solar cell structure. In order to increase

the efficiency of PV/T systems, there is a need for future studies on low-cost nanofluids with good thermal properties.

Finned Systems: Achieve higher thermal efficiency (14.73%) than finless designs (10.04%).

Nanofluids: Outperform water-based systems, with MWCNT/water leading.

Agreement with Literature: Results align with studies using similar nanofluids and configurations. Future research should focus on cost-effective nanofluids and advanced fin geometries to further boost efficiency.

Table 1. Comparison of this study with different studies in terms of system effectiveness.

Studies	Inputs	Work Fluids	Comparison of the Performance of Classical PV Systems and PV/T Systems according to Reference Systems with Different Configurations			
			$\eta_{th,\ finless}$ (%)	$\eta_{th,\ finned}$ (%)	$\varepsilon_{finless}$ (%)	ε_{finned} (%)
Alous, S., Kayfeci, M., and Uysal, A. [3]	0.5 L·min^{-1}, I_{max} = 940 W·m^{-2}	MCWNT/Water	13.6	-	-	
Fayaz, H., Nasrin, R., Rahim, N.A., *et al.* [22]	120 L·min^{-1}, I_{max} = 1000 W·m^{-2}	MCWNT/Water	12.25	-	-	-
Nasrin, R., Rahim, N.A., Fayaz, H., *et al.* [23]	0.5 L·min^{-1}, I_{max} = 1000 W·m^{-2}	MCWNT/Water	9.2	-	-	-
Hemmat Esfe, M., Kamyab, M.H., Valadkhani, M. [4]	3.73 kg·s^{-1}, I_{max} = 810.54 W·m^{-2}	Water	13.8	-	-	-
Farzanehnia, A. and Sardarabadi, M. [24]	I_{max}= 1000 - 1150 W·m^{-2}	CWWs	-	8.3		7.8
Farzanehnia, A. and Sardarabadi, M. [24]	I_{max}= 1000 - 1150 W·m^{-2}	RAFs	-	5.1		4
Lee, J.H., Hwang, S.G. and Lee, G.H. [25]	3 - 4 L·min^{-1}, I_{max} = 958.22 W·m^{-2}	CuO/Water	21.30	-	-	-
Lee, J.H., Hwang, S.G. and Lee, G.H. [25]	3 - 4 L·min^{-1}, I_{max} = 958.22 W·m^{-2}	Al_2O_3/Water	15.14	-	-	-
Prasetyo, S.D., Prabowo, A.R. and Arifin, Z. [26]	0.01 kg·s^{-1}	SiO_2	14.31	-	-	-
Gundala, S., Basha, M.M., Madhurima, V., *et al.* [27]	0.5 - 1 L·min^{-1}, I_{max} = 1017.1 W·m^{-2}	Water, Graphene/Water	26.3	-	-	-
Abdallah, S.R., Saidani-Scott, H. and Abdellatif, O.E. [19]	1.2 L·min^{-1}, I_{max} = 1000 W·m^{-2}	MCWNT/Water	26.4	-	-	-
Özakin, A.N. and Kaya, F. [18]	0.065 kg·s^{-1}, I_{max} = 1000 W·m^{-2}	Air	-	-	25	30
Sardarabadi, M., Passandideh-Fard, M., *et al.* [8]	40 L·h^{-1}, I_{max} = 921 W·m^{-2}	SiO_2 (Silica)/Water	12.8	-	24.31	-
Al-Shamani, A.N., Sopian, K., Mat, S., *et al.* [28]	0.17 kg·s^{-1}, I_{max} = 1000 W·m^{-2}	SiC/Water	12.857	-	-	-
Al-Waeli, A.H.A., Chaichan, M.T., *et al.* [29]	0.17 kg·s^{-1}, I_{max} = 1000 W·m^{-2}	SiC/Water	-	13.7	-	-

Continued

Ebaid, M.S.Y., Ghrair, A.M. and Al-Busoul, M. [30]	5 L·min^{-1}, I_{max} = 830 W·m^{-2}	$TiO_2/Al_2/O_3$/Water	-	7.67	-	-
Hosseinzadeh, M., Salari, A., *et al.* [21]	9 kg·s^{-1}, I_{max} = 830 W·m^{-2}	ZnO/Water, Pure Water	-	16.21		-
Chow, T.T. [1]	M/Ac = 75 kg·m^{-2}, I_{max} = 600 W·m^{-2}	Water	-	-	12.1	-
Present Study	5 m·s^{-1}, I_{max} = 1000 W·m^{-2}	MCWNT/Water, Graphene/Water	10.04	14.73	4.5	4.5

5. Optimization

5.1. Challenges and Objectives

PV/T systems operating without active cooling experience elevated temperature limits, leading to performance degradation and reduced operational lifespan. Non-uniform temperature distribution and thermal stress further exacerbate these issues. As demonstrated by the contours and graphs, configurations utilizing nanofluids and finned serpentines significantly improve temperature regulation, ensuring the system operates within optimal thermal ranges. The finned serpentine design enhances convective heat transfer by increasing the surface area for heat exchange between the coolant and the PV/T surface, thereby accelerating heat dissipation and lowering module temperatures. Among the tested configurations, the finned serpentine with MWCNT/water nanofluid emerges as the most effective, achieving the highest system performance.

5.2. Methodology: Taguchi and Regression Analysis

To optimize system performance, the Taguchi method was employed to identify the most efficient operating parameters. This statistical approach was complemented by a regression-based sensitivity analysis, which quantified the impact of key variables—such as flow rate, solar irradiance, and serpentine configuration—on system efficiency. In the Taguchi analysis performed using a suitable statistical program, 27 different designs were planned for each configuration, each with a level design of 4 and a number of factors of 3. Here, solar radiation values of 200, 400, 600, 800, 1000 W/m^2 were taken as design levels, respectively, while air flow rate, energy, and exergy efficiencies were selected as factor numbers (**Table 2**). The analysis revealed correlations between inputs (e.g., air velocity, solar radiation) and outputs (e.g., exergy efficiency), enabling the derivation of optimal operating conditions. Key steps are included below:

1) Model Validation: Regression equations were generated for each flow configuration to predict exergy efficiency (ε).

2) Sensitivity Analysis: Determined the relative influence of each parameter (e.g., air velocity had a stronger effect than solar radiation in finned designs).

3) Error Assessment: Achieved high reliability with coefficients of determination (R^2 > 95%) and minimal error rates (0.28% - 1.69%).

Table 2. Summary table of regression equations and performance metrics for each configuration.

Fluid	$\varepsilon_{finless}$ (%)	ε_{finned} (%)	V_{air} (m·s^{-1})	I (W·m^{-2})	R (%)	Error (%)	Multiply Regression Equation for ε_{finned} (%)
No Flow	9.89	9.94	4.36	200	96.53	1.69	$8.131-0.0110*V_{air}+0.01023*I-0.0045*V_{air}^2-0.000003*I^2+0.000050*V_{air}*I$
	11.66	11.67		400			
	13.15	13.17		600			
	14.39	14.41		800			
	15.39	15.37		1000			
Water	11.29	11.31	5	200	98.64	0.95	$9.015-0.0122*V_{air}+0.00992*I-0.0145*V_{air}^2-0.000002*I^2+0.000138*V_{air}*I$
	13.08	13.15		400			
	14.69	14.83		600			
	16.14	16.34		800			
	17.44	17.67		1000			
Graphene Nano Platelet/Water	11.31	11.41	5	200	98.8	0.28	$9.264-0.0179*V_{air}+0.00877*I+0.0095*V_{air}^2-0.000001*I^2+0.000242*V_{air}*I$
	13.17	13.24		400			
	14.89	14.96		600			
	16.45	16.58		800			
	17.87	18.09		1000			
MCWNT/Water	11.33	11.35	5	200	96.74	0.69	$9.500-0.0380*V_{air}+0.00961*I+0.0042*V_{air}^2-0.000002*I^2+0.000300*V_{air}*I$
	13.27	13.34		400			
	15.05	15.18		600			
	16.68	16.87		800			
	18.15	18.4		1000			

6. Discussion

6.1. Optimization Results

Optimization provides additional contributions to the precise determination of the optimum operating conditions for PV/T systems, the validation of CFD and thermodynamics analysis results. The statistical study also minimizes the complexity of the mathematical model by reducing the number of variables in the optimization process.

The temperature limits of the PVT system operating without any cooling increase, which leads to potential performance loss. Technically, the non-uniform temperature distribution, together with thermal stress, negatively affects the performance and operational life of the system. The temperature of the modules plays an important role in determining the module efficiency. Looking at the contours and graphs, it is clear that the nanofluid and finned serpentine configurations provide better results in reducing PVT system temperatures to ideal temperatures. The finned serpentine used improves the convective heat transfer rate by increas-

ing the heat exchange surface area between the coolant and the PVT surface. This improvement enables faster heat removal from the PVT modules and ensures lower operating temperatures. Generally, it is understood that the PVT system with fins and MNCWNT nanofluid has the most effective system performance. As can be seen from the figures, when the solar radiation increases from 200 [W·m^{-2}] to 1000 [W·m^{-2}], the cooling fluid temperatures also increase.

Finned vs. Finless: Finned serpentines consistently outperformed finless designs, with exergy efficiency improvements of up to 18.4% for MWCNT/water at 1000 W/m^2 and 5 m·s^{-1} air velocity.

Nanofluid Superiority: MWCNT/water nanofluid yielded the highest efficiency due to its superior thermal conductivity, followed by graphene nano platelets and water.

Key Parameters:

Air velocity (V_{air}): Higher velocities (5 m·s^{-1}) enhanced cooling but required balancing against pumping power costs.

Solar radiation (I): Efficiency scaled with irradiance, though temperature management became critical at 1000 [W·m^{-2}].

Sample Regression Equation for MWCNT/Water (Finned):

$$\mathcal{E}_{finned} = 9500 - 0.0380 * V_{air} + 0.00961 * I + 0.0042 * V_{air}^2 - 0.000002 * I^2 + 0.000300 * V_{air} * I$$

6.2. Practical Implications

6.2.1. Design Recommendations

Prioritize finned serpentines with MWCNT/water nanofluid for maximal efficiency.

Optimize air velocity to [5 m·s^{-1}] for high-irradiance conditions (≥800 W·m^{-2}).

6.2.2. Future Work

Explore low-cost nanofluids with comparable thermal properties.

Investigate hybrid cooling systems (e.g., nanofluids + phase-change materials).

6.3. Key Findings and Performance Improvements

As the performance of PV/T systems increases by around 30% at ideal cell temperatures, the addition of a suitable cooling system and the selection of the working fluid are important design criteria for such systems. Through computational fluid dynamics (CFD) and thermodynamic analyses, conducted using Ansys Fluent. This study evaluated designs to enhance PV/T system efficiency. Key results include:

Finned Serpentine Superiority: Achieved a 10% increase in total energy efficiency and a 0.5% rise in exergy efficiency compared to finless designs.

Nanofluid Performance: The MWCNT/water mixture delivered the highest performance, outperforming graphene nano-pellet/water and pure water by 5% in energy efficiency and 0.4% in exergy efficiency.

Airflow Impact: Higher air velocities consistently improved both energy and exergy efficiencies across all configurations.

6.4. Proposed Design Enhancements

To further optimize PV/T systems, the following steps are recommended.

6.4.1. Advanced Serpentine and Fin Designs

Develop more compact and aerodynamically efficient serpentine geometries to maximize heat transfer surface area.

Explore multi-fin arrangements or graded fin densities to address localized hot spots.

6.4.2. Nanofluid Innovation

To improve the efficiency of PV/T systems, a PV/T system with and without fins and a serpentine type heat exchanger was analyzed, and the use of nanofluids at a concentration of 0.5%, water, and air circulation at different velocities from the external surface was also considered.

Experiment with hybrid nanofluids (e.g., MWCNT + graphene) to synergize thermal properties.

Investigate cost-effective alternatives (e.g., oxide-based nanofluids) without compromising performance.

6.4.3. Experimental Validation

Validate CFD results with real-world prototypes to bridge the gap between simulation and practical performance. Conduct long-term durability tests to assess nanofluid stability and system degradation.

7. Conclusions

This study investigated the thermal and exergetic performance of a PV/T system enhanced with internal fins and nanofluids under varying air velocities and solar irradiance. CFD simulations combined with Taguchi optimization and regression analysis provided valuable insights into how different configurations influence energy conversion efficiency.

Finned serpentine channels significantly improved both energy and exergy efficiencies compared to finless designs—by up to 10% and 0.5%, respectively—due to increased heat transfer surface area [18].

Among the tested fluids, MWCNT/water nanofluid achieved the highest overall performance, with up to 18.4% exergy efficiency at 1000 [$W \cdot m^{-2}$] and 5 [$m \cdot s^{-1}$] air velocity. This aligns with previous studies highlighting the superior thermal conductivity of MWCNTs [3] [19].

Higher air velocities consistently improved cooling effectiveness and system output, though practical limitations such as fan power and noise must be considered [20].

The integration of CFD analysis, surface modification, and advanced fluids has proven effective in optimizing PV/T system performance. The proposed finned configuration with MWCNT/water nanofluid under high air velocity is recommended for future PV/T designs. These findings are consistent with prior research

emphasizing the importance of fluid selection and heat exchanger design in enhancing PV/T system efficiency [18] [21].

One of the fundamental criteria in the design of the air-source, finned serpentine heat exchanger used in the PV/T system is ensuring minimum fan power and pressure drop values. The optimal design of this type of heat exchangers is based on a certain number of geometrical and operational parameters. As is known, an optimization design starts by selecting criteria to minimize or maximize, which is called an objective function. In an optimization design, the requirements of a particular design, such as required heat transfer, allowable pressure drop, and fan power, are calculated accordingly, along with other constraints. Therefore, to overcome these requirements, advanced optimization algorithms such as the genetic algorithm are developed, which are gradient-free.

This study focuses on the cooling system and working fluids that improve the thermal performance of PVT systems for operation under ideal conditions; however, the fan power providing the secondary fluid air flow and the pressure drop in the flow medium have not been calculated. In more comprehensive analyses, the role of these two parameters in the operation of the system, especially under economic conditions, should be investigated.

Even if the pressure drop and fan power requirements for the secondary fluid air in the analyzed system are quite low, they can become quite significant for PV/T power plants, leading to a significant increase in energy consumption and a reduction in overall performance. In the literature, optimization studies of excessive pressure drop across serpentine can aim for air flow without excessive power use. Similarly, minimizing fan power and pressure drop have shown improvements; these must be carefully designed to provide optimal size and capacity. To balance this capacity/size ratio, fan systems can be geometrically reduced in size by approximately 4% to 10% [31] [32].

Future work should focus on cost-effective nanofluid alternatives, hybrid cooling methods (e.g., nanofluids with PCMs), and experimental validation under real environmental conditions. Researchers working on PV/T systems, a renewable energy source, should focus on analyses aimed at developing well-designed cooling heat exchangers and working nanofluids, and bring high-efficiency systems to industry through advanced analysis techniques and algorithms.

Conflicts of Interest

The authors declare no conflicts of interest regarding the publication of this paper.

References

[1] Chow, T.T. (2010) A Review on Photovoltaic/Thermal Hybrid Solar Technology. *Applied Energy*, **87**, 365-379. https://doi.org/10.1016/j.apenergy.2009.06.037

[2] Kalogirou, S.A. (2023) Solar Energy Engineering: Processes and Systems. Academic Press.

[3] Alous, S., Kayfeci, M. and Uysal, A. (2019) Experimental Investigations of Using MWCNTS and Graphene Nanoplatelets Water-Based Nanofluids as Coolants in PVT

Systems. *Applied Thermal Engineering*, **162**, Article 114265. https://doi.org/10.1016/j.applthermaleng.2019.114265

[4] Hemmat Esfe, M., Kamyab, M.H. and Valadkhani, M. (2020) Application of Nanofluids and Fluids in Photovoltaic Thermal System: An Updated Review. *Solar Energy*, **199**, 796-818. https://doi.org/10.1016/j.solener.2020.01.015

[5] Meneses-Rodríguez, D., Horley, P.P., González-Hernández, J., Vorobiev, Y.V. and Gorley, P.N. (2005) Photovoltaic Solar Cells Performance at Elevated Temperatures. *Solar Energy*, **78**, 243-250. https://doi.org/10.1016/j.solener.2004.05.016

[6] Sachit, F.A., Rosli, M.A.M., Tamaldin, N., Misha, S. and Abdullah, A.L. (2018) Nanofluids Used in Photovoltaic Thermal (PV/T) Systems: A Review. *International Journal of Engineering & Technology*, **7**, 599-611. https://www.researchgate.net/public./328802644

[7] Qeays, I.A., Yahya, S.M., Arif, M.S.B. and Jamil, A. (2020) Nanofluids Application in Hybrid Photovoltaic Thermal System for Performance Enhancement: A Review. *AIMS Energy*, **8**, 365-393. https://doi.org/10.3934/energy.2020.3.365

[8] Sardarabadi, M., Passandideh-Fard, M. and Zeinali Heris, S. (2014) Experimental Investigation of the Effects of Silica/water Nanofluid on PV/T (Photovoltaic Thermal Units). *Energy*, **66**, 264-272. https://doi.org/10.1016/j.energy.2014.01.102

[9] Hamoudah, K.S., Etaig, S. and Elabeedy, E. (2025) Enhance Photovoltaic/Thermal (PV/T) System Performance by Using Nanofluid. *Solar Energy and Sustainable Development Journal*, **14**, 17-35. https://doi.org/10.51646/jsesd.v14ificts-2024.441

[10] Samylingam, L., Aslfattahi, N., Saidur, R., Yahya, S.M., *et al.* (2021) Performance Prediction and Optimization of Nanofluid-Based PV/T Using Numerical Simulation and Response Surface Methodology. *Nanomaterials*, **14**, Article 774.

[11] El Hadi Attia, M., Kabeel, A.E., Khelifa, A., Abdelgaied, M., *et al.* (2023) Performance Enhancement of PVT Modules Using Bi Fluid (Air/CuO-Water Based Nanofluid) and Fins: Energy and Exergy Analysis. *Clean Technologies and Environmental Policy*, **27**, 4541-4559.

[12] Versteeg, H.K. and Malalasekera, W. (1995) An Introduction to Computational Fluid Dynamics: The Finite Volume Method. Pearson Education Ltd.

[13] User Guide (2019) Simcenter STAR-CCM+ Documentation Version 2019.3, Siemens PLM Software.

[14] Cebeci, T., Shao, J.P., Kafyeke, F. and Laurendeau, E. (1995) Computational Fluid Dynamics for Engineers. Horizon Research Publishing.

[15] Gökçe, M.K. (2020) Gemi Özitme Parametrelerinin Sayısal ve Deneysel Olarak Hesaplanması. Doktora Tezi, Yıldız Teknik Üniversitesi.

[16] Hu, C. and White, R.M. (1983) Solar Cells: From Basic to Advanced Systems. McGraw-Hill.

[17] Jeter, S.M. (1981) Maximum Conversion Efficiency for the Utilization of Direct Solar Radiation. *Solar Energy*, **26**, 231-236. https://doi.org/10.1016/0038-092x(81)90207-3

[18] Özakin, A.N. and Kaya, F. (2019) Effect on the Exergy of the PVT System of Fins Added to an Air-Cooled Channel: A Study on Temperature and Air Velocity with ANSYS Fluent. *Solar Energy*, **184**, 561-569. https://doi.org/10.1016/j.solener.2019.03.100

[19] Abdallah, S.R., Saidani-Scott, H. and Abdellatif, O.E. (2019) Performance Analysis for Hybrid PV/T System Using Low Concentration MWCNT (Water-Based) Nanofluid. *Solar Energy*, **181**, 108-115. https://doi.org/10.1016/j.solener.2019.01.088

[20] Bosanac, M., Sorensen, B., Katic, I., Sorensen, H., Nielsen, B. and Badran, J. (2003) Photovoltaic/Thermal Solar Collectors and Their Potential in Denmark. EFP Project 1713/00-0014, Final Report.

[21] Hosseinzadeh, M., Salari, A., Sardarabadi, M. and Passandideh-Fard, M. (2018) Optimization and Parametric Analysis of a Nanofluid Based Photovoltaic Thermal System: 3D Numerical Model with Experimental Validation. *Energy Conversion and Management*, **160**, 93-108. https://doi.org/10.1016/j.enconman.2018.01.006

[22] Fayaz, H., Nasrin, R., Rahim, N.A. and Hasanuzzaman, M. (2018) Energy and Exergy Analysis of the PVT System: Effect of Nanofluid Flow Rate. *Solar Energy*, **169**, 217-230. https://doi.org/10.1016/j.solener.2018.05.004

[23] Nasrin, R., Rahim, N.A., Fayaz, H. and Hasanuzzaman, M. (2018) Water/MWCNT Nanofluid Based Cooling System of PVT: Experimental and Numerical Research. *Renewable Energy*, **121**, 286-300. https://doi.org/10.1016/j.renene.2018.01.014

[24] Farzanehnia, A. and Sardarabadi, M. (2019) Exergy in Photovoltaic/Thermal Nanofluid-Based Collector Systems. In: *Exergy and Its Application—Toward Green Energy Production and Sustainable Environment*, Intech Open, 1-3. https://doi.org/10.5772/intechopen.85431

[25] Lee, J.H., Hwang, S.G. and Lee, G.H. (2019) Efficiency Improvement of a Photovoltaic Thermal (PVT) System Using Nanofluids. *Energies*, **12**, Article 3063. https://doi.org/10.3390/en12163063

[26] Prasetyo, S.D., Prabowo, A.R. and Arifin, Z. (2022) Investigation of Thermal Collector Nanofluids to Increase the Efficiency of Photovoltaic Solar Cells. *International Journal of Heat and Technology*, **40**, 415-422. https://doi.org/10.18280/ijht.400208

[27] Gundala, S., Basha, M.M., Madhurima, V., Praveena, N. and Kumar, S.V. (2021) An Experimental Performance on Solar Photovoltaic Thermal Collector with Nanofluids for Sustainable Development. *Journal of Nanomaterials*, **2021**, 1-6. https://doi.org/10.1155/2021/6946540

[28] Al-Shamani, A.N., Sopian, K., Mat, S., Hasan, H.A., Abed, A.M. and Ruslan, M.H. (2016) Experimental Studies of Rectangular Tube Absorber Photovoltaic Thermal Collector with Various Types of Nanofluids under the Tropical Climate Conditions. *Energy Conversion and Management*, **124**, 528-542. https://doi.org/10.1016/j.enconman.2016.07.052

[29] Al-Waeli, A.H.A., Chaichan, M.T., Kazem, H.A. and Sopian, K. (2017) Comparative Study to Use Nano-(Al_2O_3, CuO, and SiC) with Water to Enhance Photovoltaic Thermal PV/T Collectors. *Energy Conversion and Management*, **148**, 963-973. https://doi.org/10.1016/j.enconman.2017.06.072

[30] Ebaid, M.S.Y., Ghrair, A.M. and Al-Busoul, M. (2018) Experimental Investigation of Cooling Photovoltaic (PV) Panels Using (TiO_2) Nanofluid in Water-Polyethylene Glycol Mixture and (Al_2O_3) Nanofluid in Water-Cetyltrimethylammonium Bromide Mixture. *Energy Conversion and Management*, **155**, 324-343. https://doi.org/10.1016/j.enconman.2017.10.074

[31] Mao, J.B., Ma, X.J., Zhao, F., Wang, G.J., *et al.* (2023) A Novel Design to Enhance the Heat Transfer and Reduce Pressure Drop of Heat Exchangers Based on Multi-Objective Optimization. *Jurnal Ilmiah Teknik Sipil dan Teknik Kimia*, **8**, 128-139.

[32] Ni'mah, K.P., Fitriah and Sari, D.A. (2023) [Evaluasi Kinerja Air-Cooled Heat Exchanger Pada Unit Pemisahan Berdasarkan Fouling Factor dan Pressure Drop]. *Jurnal Ilmiah Teknik Sipil dan Teknik Kimia*, **8**, 128-139. https://doi.org/10.33366/rekabuana.v8i2.4951